Research in Astronomy and Astrophysics manuscript no.
(LaTeX: cliu˙raa˙revised.tex; printed on March 28, 2013; 21:17)

Triggering of star formation by both radiative and mechanical AGN feedback *

Chao Liu[1,2], Zhao-ming Gan[1], Fu-guo Xie[1]

[1] Key Laboratory for Research in Galaxies and Cosmology, Shanghai Astronomical Observatory, Chinese Academy of Sciences, 80 Nandan Road, Shanghai 200030, China; *cliu@shao.ac.cn*

[2] University of Chinese Academy of Sciences, 19A Yuquan Road, Beijing 100049, China

Received 2012 xx; accepted xx xx

Abstract We perform two dimensional (2D) hydrodynamic (HD) numerical simulations to study the positive active galaxy nuclei (AGN) feedback which triggers, rather than suppresses, star formation. Recently, it is shown by Nayakshin et al. (2012) and Ishibashi et al. (2012) that star formation occurs when the cold interstellar medium (ISM) is squeezed by the impact of mass outflow or radiation pressure, respectively. Mass outflow is ubiquitous in this astrophysical context, and radiation pressure is also important if the AGN is luminous. For the first time on this subject, we take both mass outflow feedback and radiative feedback into our model. Consequently, the ISM is shocked into shells by the AGN feedback, and then these shells fragment into clumps and filaments very soon because of the Rayleigh-Taylor and thermal instabilities. We have two major findings in this paper: (1) the star formation rate (SFR) can indeed be very large in the clumps and filaments. However, the resultant star formation rate density (SFRD) is somehow too large compared to previous works, which is mainly due to that we ignore that most of the formed stars would be disrupted when they pass away from the galaxy center; (2) although radiation pressure feedback has limited effect, when mass outflow feedback is also included, they reinforce each other. Specifically, in the gas-poor case, mass outflow is always the dominant feedback contributor.

Key words: methods: numerical — accretion — shock waves — galaxies: active — galaxies: starburst

1 INTRODUCTION

The observed correlations between the mass of the central supermassive black hole (SMBH) and the characteristic properties of the host galaxy (Gebhardt et al. 2000; Ferrarese & Merritt 2000; Marconi & Hunt 2003; Fabian 2012) indicate that AGN feedback is likely to play an important role in the galaxy formation

and evolution (Silk & Rees 1998; Proga et al. 2000; Di Matteo et al. 2005; Ciotti et al. 2009; Kurosawa & Proga 2009; Fanidakis et al. 2011). AGN can influence its environment and/or its host galaxy in various forms, i.e., radiation pressure, radiative heating, jets and winds/outflows. Jets are believed to be responsible for the formation of the X-ray cavities observed in the clusters of galaxies (e.g., Fabian et al. 2006). Since the jets are highly collimated, they are prone to drill through a single galaxy. It is reasonable to ignore the jet feedback in this work, because we focus on the galactic enter of several kilo-parsecs in a single galaxy.

In the traditional view, it is believed that the AGN feedback impacts its host galaxy in a negative way. Namely, the ISM around the SMBH is heated up by photoexcitation/photoionization and Compton heating; or it is blown away by radiation pressure and ram pressure of mass outflows. It is believed that these processes inhibit the star formation and the gas fueling onto the SMBH (e.g., Springel et al. 2005; Farrah et al. 2012; Cano-Díaz et al. 2012; Page et al. 2012). However, the feedback might be positive in terms of triggering star formation in the host galaxy (Fabian 2012). Santini et al. (2012) reported evidences of a higher average star formation activity in AGN hosts with respect to a control sample of inactive galaxies. The level of star formation enhancement is modest (~ 0.26 dex at $\sim 3\sigma$ confidence level) at low X-ray luminosity ($L_X \lesssim 10^{43.5}$ erg s^{-1}) and more pronounced (0.56 dex at $> 10\sigma$ confidence level) in the hosts of luminous AGNs. In another interesting work, Silk & Nusser (2010) proposed that the outflow triggered star formation can help to boost the momentum rate from L_{acc}/c released by AGN radiation to $\sim 2-30\ L_{acc}/c$ deposited into the galactic winds (e.g., Moe et al. 2009; Sturm et al. 2011), where L_{acc} is the AGN accretion luminosity and c is the speed of light.

More recently, there are two theoretical works focused on the physical processes of positive AGN feedback. One is done by Nayakshin & Zubovas (2012), they did smoothed-particle hydrodynamics (SPH) simulation of quasar feedback on a gas shell and found that when the ambient shocked gas cools rapidly, the shocked gas is compressed into thin cold dense shells, filaments and clumps. Some of these high density features are found to be resilient to the feedback, so they are hotbed for starburst. In their work, they considered only mass outflow feedback by assuming wind velocity $v_w = 0.1\ c$ and wind momentum rate $\dot{p}_w = L_{Edd}/c$, where L_{Edd} is the Eddington luminosity. The other one is an analytic work done by Ishibashi & Fabian (2012), they found that the squeezing and compression of the inhomogeneous interstellar medium can trigger star formation within the radiation pressure-driven dusty gas shell when the shell expanding outward. They explored the shell's escape/trapping condition in the galactic halo for different underlying dark matter potentials. In their picture, new stars form at increasingly larger radii and successively populate the outer regions of the host galaxy. This inside-out growth pattern seems to match the observational fact that the increase in stellar mass mainly occurs at outer radii since redshift z≈2 (van Dokkum et al. 2010) just after quasar activity had peaked.

The main purpose of this paper is to study the possibility of star formation triggered by AGN feedback through grid-based HD simulations. Our main improvement is to include both mass outflow and radiative feedbacks in our models. We note that although Nayakshin & Zubovas (2012) studied the quasar feedback, but radiative feedback such as radiative heating and radiation pressure is ignored. However, quasars are so luminous that radiative feedback is the dominated feedback, which is usually referred as quasar mode

of Ishibashi & Fabian (2012) who considered only radiation pressure on dust. We ignored dust opacity in our models. Instead, we take into account line-force and Thomson scattering to calculate the radiative feedback force. In addition, we take a more complete treatment of radiative heating/cooling while there is only bremsstrahlung in Nayakshin & Zubovas (2012) and no radiative heating/cooling in Ishibashi & Fabian (2012). We aim at investigating the positive AGN feedback under our improved models.

In the following section, we describe our modeling of AGN feedback mechanisms, numerical methods and model assumptions. We analyze the results of our HD numerical simulations in Section 3. Finally, we make conclusion and discussions in Section 4.

2 METHOD

We focus on the inner part of an isolated galaxy in order to reach a relatively higher resolution. The central engine is treated as a point source composed of two components, an accretion disc radiates at ultraviolet (UV) band where its flux is proportional to $cos(\theta)$ and a corona radiating at X-ray band isotropically. The radiative heating/cooling mechanisms include Compton heating/cooling, X-ray photoionization heating/recombination cooling, bremsstrahlung and line cooling (Proga et al. 2000). We model the galaxy with a singular isothermal sphere with the total density profile $\rho = \sigma^2/(2\pi G r^2)$, where σ is the velocity dispersion and G is the gravitational constant. Correspondingly, the acceleration of the gravity is

$$\mathbf{g}^{*,DM} = -\frac{2\sigma^2}{r^2}. \tag{1}$$

The gas density is assumed to be a fraction f_g of the total density, i.e., $\rho_g = f_g\sigma^2/(2\pi G r^2)$. Then, the gas mass enclosed in r is $M_g = 4\pi \int \rho_g r^2 dr = 2 f_g \sigma^2 r/G$.

2.1 AGN feedback Model

Both radiative feedback and mechanical feedback are considered. In terms of the radiative feedback, we follow the treatments of Proga et al. (2000). The radiative heating/cooling and radiation pressure is added to the energy and momentum equations as source terms, respectively. The radiation pressure is taken into account through Thomson scattering and line-force, where the line-force is parameterized by a line-force multiplier (Stevens & Kallman 1990, see also Proga et al. 2000). The acceleration as a result of radiation pressure can be written as

$$\mathbf{g}^{rad}(r,\theta) = \frac{\kappa_{es}}{c}\frac{L_{acc}}{4\pi r^2}\left[f_* \exp\left(-\tau_X\right) + (1+\mathcal{M}) \times 2\left|\cos\theta\right| f_d \exp\left(-\tau_{UV}\right)\right] \cdot \hat{\mathbf{r}}, \tag{2}$$

where $\kappa_{es} = 0.4\,\mathrm{cm^2\ g^{-1}}$ is the mass-scattering coefficient for free electrons, $\mathcal{M}$ is the line-force multiplier, L_{acc} is the accretion luminosity ($L_{acc} = \epsilon_{EM}\dot{M}_{acc}c^2$, where $\dot{M}_{acc}$ is the BH mass accretion rate and ϵ_{EM} is the radiation efficiency), f_* and f_d respectively are the X-ray and UV flux fraction, τ_X and τ_{UV} respectively are the X-ray and UV optical depth. We assume the ISM is optically thin to its own radiation and the UV radiation from the central engine. Therefore, there is only the radial component in the equation (2) and $\tau_{UV} = 0$.

Considering a gas shell under the irradiation of the central engine with luminosity L_{acc}, one can get

force, which leads to

$$L_c = \frac{4 f_g c \sigma^4}{G} = 4.6 \times 10^{46} \left(\frac{f_g}{0.16}\right) \left(\frac{\sigma}{2 \times 10^7 \mathrm{cm/s}}\right)^4 \mathrm{ergs\,s^{-1}}. \quad (3)$$

When $L_{acc} > L_c$, the gas shell will be blown away. For simplicity, we set $L_{acc} = L_c$ throughout the current work. If we set the mass of SMBH $M_{BH} = 10^8 M_\odot$, $\sigma = 200$ km s^{-1} and $f_g = 0.16$ (gas-rich case), we immediately have $L_{acc} \simeq 3.5 L_{Edd}$. But for $f_g = 10^{-3}$ (gas-poor case), the accretion luminosity is as low as $L_{acc} \simeq 2.2\% L_{Edd}$.

For the mechanical feedback, we consider fast mass outflow with outward radial velocity fixed to $v_w = 10000$ km/s. There are many compelling observational evidences for the existence of fast outflows (e.g., Crenshaw 1997; Kaastra et al. 2000; Hamann et al. 1997; Chartas et al. 2003; Crenshaw et al. 2003; Hamann et al. 2008; Tombesi et al. 2010, 2011, 2012). We add outflows mass, momentum and kinetic energy as source terms to the basic HD equations at the innermost layer (similar to the treatments by Ostriker et al. 2010). The mass outflow rate $\dot{M}_w$, outflow momentum rate $\dot{P}_w$ and kinetic energy rate $\dot{E}_w$ are calculated as follows:

$$\dot{M}_w = \eta_w \frac{L_{acc}}{c} \frac{1}{v_w}, \quad (4)$$

$$\dot{P}_w = \dot{M}_w v_w = \eta_w \frac{L_{acc}}{c}, \quad (5)$$

$$\dot{E}_w = \frac{1}{2} \dot{M}_w v_w^2 = \epsilon_w \dot{M}_{acc} c^2, \quad (6)$$

where ϵ_w is wind/outflow efficiency and η_w is the ratio of mass outflow momentum rate over radiation momentum rate. The definition of η_w can be derived from equations (5) and (6),

$$\eta_w \equiv 2 \frac{\epsilon_w}{\epsilon_{EM}} \frac{c}{v_w}. \quad (7)$$

The radiation efficiency ϵ_{EM} is set to be 0.1 throughout this paper. The wind/outflow efficiency is not well constrained yet, the best estimation is in the range $1 \times 10^{-3} > \epsilon_w > 3 \times 10^{-4}$ (Proga et al. 2000; Proga & Kallman 2004; Krongold et al. 2007; Kurosawa & Proga 2009; Ostriker et al. 2010). If we set $\epsilon_w = 5 \times 10^{-3}$, then $\eta_w = 3$. The outflowing mass flux is also assumed to be dependent on the angle from the polar axis as $\propto \frac{3}{2} sin\theta cos^2\theta$, so that the half-opening angle enclosing half of the input material is $\approx 45^\circ$. In terms of solid angle, this means that the wind is visible from about $1/4$ of the available viewing angles.

2.2 Numerical Setup

We perform 2D HD numerical simulations with the modified code ZEUS-MP (Stone & Norman 1992; Hayes et al. 2006) in the spherical polar coordinates (r, θ, ϕ). The equations including feedback source terms are:

$$\frac{D\rho}{Dt} + \rho \nabla \cdot \mathbf{v} = 0, \quad (8)$$

$$\rho \frac{D\mathbf{v}}{Dt} = -\nabla P + \rho \mathbf{g} + \rho \mathbf{g}^{\mathrm{rad}}, \quad (9)$$

$$\rho \frac{D}{Dt}\left(\frac{e}{\rho}\right) = -p \nabla \cdot \mathbf{v} + \rho \mathcal{L}, \quad (10)$$

where ρ is the mass density, P is the gas pressure, $\mathbf{v}$ is the velocity, e is the internal energy density, $\rho\mathcal{L}$

Table 1 Model summary

Model Number	Model	f_g [a]	ϵ_w [b]	Radiation Pressure Feedback	Outflow Feedback	t_{kpc} [c] Myr
1	AMR	0.16	5×10^{-3}	$\surd$	$\surd$	1.92
2	AR	0.16	5×10^{-3}	$\surd$	$\times$	No
3	AM	0.16	5×10^{-3}	$\times$	$\surd$	2.37
4	BMR	10^{-2}	5×10^{-3}	$\surd$	$\surd$	2.91
5	BR	10^{-2}	5×10^{-3}	$\surd$	$\times$	No
6	BM	10^{-2}	5×10^{-3}	$\times$	$\surd$	3.04
7	CMR	10^{-3}	5×10^{-3}	$\surd$	$\surd$	1.79
8	CR	10^{-3}	5×10^{-3}	$\surd$	$\times$	No
9	CM	10^{-3}	5×10^{-3}	$\times$	$\surd$	1.79

Notes: The model names indicate different physics. A, B, C indicates different f_g; M means mass outflow feedback; R means radiation pressure feedback. a: f_g is the gas fraction. b: ϵ_w is the wind efficiency. c: the time when the outer shell first arrives at $r = 1$ kpc; 'No' means never.

the SMBH, dark matter and stars (i.e., $g = GM_{BH}/r + g^{*,DM}$), $\mathbf{g}^{\rm rad}$ is the acceleration due to radiation pressure (see equation (2)). The outflow feedback terms are not present in the above equations, instead, the mass, momentum and energy of the outflow are directly added to the innermost layer of our simulation domain. We adopt an adiabatic equation of state $P = (\gamma-1)e$, and consider only models with the adiabatic index $\gamma = 5/3$.

Our simulation domain covers from 5pc to 5kpc in the radial direction and from 0 to π in the angular direction. There are 192 radial grids in which $(\Delta r)_{i+1}/(\Delta r)_i = 10^{1/(N_r-1)}$, N_r denotes grid points per decade in radius. We set $N_r = 64$ here. In order to better resolve the flow near the equator, we adopt angular zones with $(\Delta\theta)_{j+1}/(\Delta\theta)_j = 0.985$ for $0 \leqslant \theta \leqslant \pi/2$, and $(\Delta\theta)_j/(\Delta\theta)_{j+1} = 0.985$ for $\pi/2 \leqslant \theta \leqslant \pi$. The outflow boundary condition is adopted at the outer radial boundary. We use the same boundary condition as Novak et al. (2011) at the inner radial boundary, i.e., assuming reflecting boundary conditions if the innermost radial velocity is positive. If the innermost radial velocity is negative, we use an outflow boundary condition where all fluid variables are constant across the boundary. In the angular direction, symmetrical boundary condition is applied at the polar axes.

3 RESULTS

The gravity of the SMBH is only effective in the innermost regions. We set the mass of the SMBH $M_{BH} = 10^8 \mathrm{M}_\odot$ and the velocity dispersion $\sigma = 200\ \mathrm{km\ s^{-1}}$, which is in consistent with the $M_{BH} - \sigma$ relation (see e.g., Ferrarese & Merritt 2000). We assume the X-ray flux fraction $f_* = 0.05$ and the UV flux fraction $f_d = 1 - f_* = 0.95$. The gas fraction f_g is taken as a free parameter. We calculated models with various f_g and with each feedback terms turned on/off. The models are summarized in Table 1. The gas fractions are given in Column 3 and the wind efficiencies are given in Column 4. The symbols "$\surd$ / $\times$" shown in Columns 5 and 6 indicate whether radiation pressure or mass outflow feedback is considered in the simulations. The

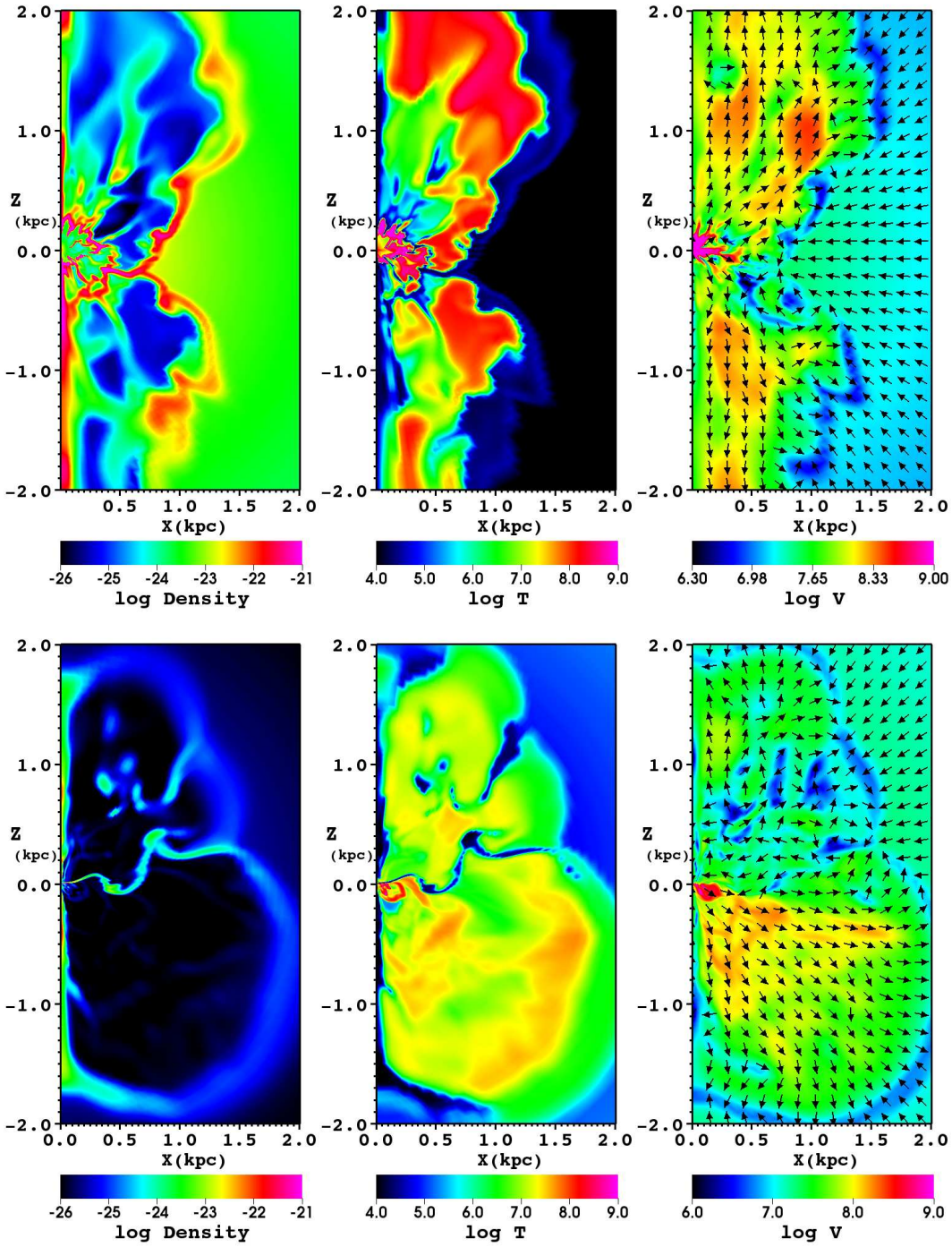

Fig. 1 Top panels: gas-rich model AMR; bottom panels: gas-poor model CMR. From the left to right columns, they are gas density ($\mathrm{g\,cm^{-3}}$), temperature (K) and velocity magnitude ($\mathrm{cm\ s^{-1}}$), respectively. The arrows in the right columns present the direction of velocities. All the panels are snapshots taken at $t = 4.47$ Myr. The cold dense clumps and filaments in model AMR are regions with high SFR. These clumps and filaments in which stars form are generated due to Rayleigh-Taylor and thermal instabilities. Most of the stars formed in the clumps and filaments are disrupted when passing away from the center. There are also clumps and filaments appear in gas-poor model CMR, this is a new result. See the text for details.

3.1 Triggering of star formation

Figure 1 shows the density (left column) and temperature (right column) contours of the ambient gas shocked by the mass outflow and radiation pressure. The top panels corresponding to the gas-rich model AMR ($f_g = 0.16$), and the bottom panels are for the gas-poor model CMR ($f_g = 10^{-3}$). From the left to right columns, they are logarithmic gas density, temperature and velocity magnitude, respectively. The arrows in the right columns present the directions of velocities. All of the panels in Figure 1 are snapshots taken at time $t = 4.47$ Myr. Under the impact of radiation pressure and ram pressure of the mass outflows, the inner interstellar medium is shocked into shells. Some of these shells fragment into clumps and filaments due to the Rayleigh-Taylor and thermal instabilities (cf. thin shell instability, it occurs when the radiative cooling is very strong, see Vishniac 1983 and also Mac Low et al. 1989). The clumps and filaments can be found easily in the left and middle panels, they have the highest density and lowest temperature. This phenomenon was also found by Nayakshin & Zubovas (2012). The cold dense clumps, filaments and shells are the ideal places for star formation. We use a simple prescription to evaluate the SFR as adopted by Ishibashi & Fabian (2012), the formula is:

$$\dot{M}_* \sim \epsilon_* \frac{M_g}{t_{flow}} \sim \epsilon_* \frac{2 f_g \sigma^2}{G} v(\mathbf{r}), \tag{11}$$

where ϵ_* is the star formation efficiency, M_g is the gas mass and $t_{flow} = r/v(\mathbf{r})$ is the local flow time. The observed star formation efficiency $\epsilon_* \sim 0.01 - 0.1$. For model AMR, we get the SFR at large radii $\dot{M}_{*,\infty} \sim 7.2 \times 10^{0-1}$ $\mathrm{M_\odot yr^{-1}}$ if $v_\infty = 60$ $\mathrm{km\,s^{-1}}$ (see top-left panel of Figure 1). By analogy, we estimate the SFRD by using the formula $\dot{\rho}_* \sim \epsilon_* \rho / t_{flow}$. The radial profiles of angle-averaged $\dot{\rho}_*/\epsilon_*$ are plotted in Figure 2 for models AMR (left panel) and CMR (right panel) with the solid, dotted and green lines corresponding to the snapshots taken at t=2.235, 4.47 and 6.705 Myr, respectively. The vertical axis is unit of $\mathrm{M_\odot yr^{-1}(100pc)^{-3}}$. From the left panel, we get the SFRD around 1 kpc at 4.47 Myr is $\sim 10^{-4}\epsilon_*$ $\mathrm{M_\odot yr^{-1}(100pc)^{-3}} = 10^6(\epsilon_*/0.01)$ $\mathrm{M_\odot yr^{-1}(Mpc)^{-3}}$. The largest SFRD in the cosmological simulations including AGN feedback presented by Fanidakis et al. (2012) is ~ 0.1 $\mathrm{M_\odot yr^{-1}(Mpc)^{-3}}$ (see their Figure 1), which is several orders of magnitude smaller than our estimation. The inconsistent is caused by several reasons. One of the most important reason is that we ignore that most of the protostars and formed stars will be disrupted when the clumps, filaments and shells passing away from the center of the galaxy (Nayakshin & Zubovas 2012). Another reason is that we get the SFRD from our simulation domain that only covers the galactic center, while the SFR is usually inversely proportional to the radius, so that the SFRD will inevitably be overestimated if we extrapolate our results to large scale directly. The details will be studied in a more accurate way in the future.

There are also clumps and filaments appeared in gas-poor model CMR, this is a new result which was not found by Nayakshin & Zubovas (2012). This is because we have line radiation pressure and more complete radiative heating/cooling, the shell instability occurs although it is much weak for gas-poor case. The consequent SFRD is much smaller compared with the gas-rich case (see the right panel of Figure 2). For example, the SFRD around 1 kpc at 4.47 Myr is $\sim 10^{-5}\epsilon_*$ $\mathrm{M_\odot yr^{-1}(100pc)^{-3}}$, which is one order of magnitude smaller than the gas rich case. On the other hand, since the feedback is weaker when the ambient gas density is smaller under our model construction, the outward velocity of the gas shell is much smaller

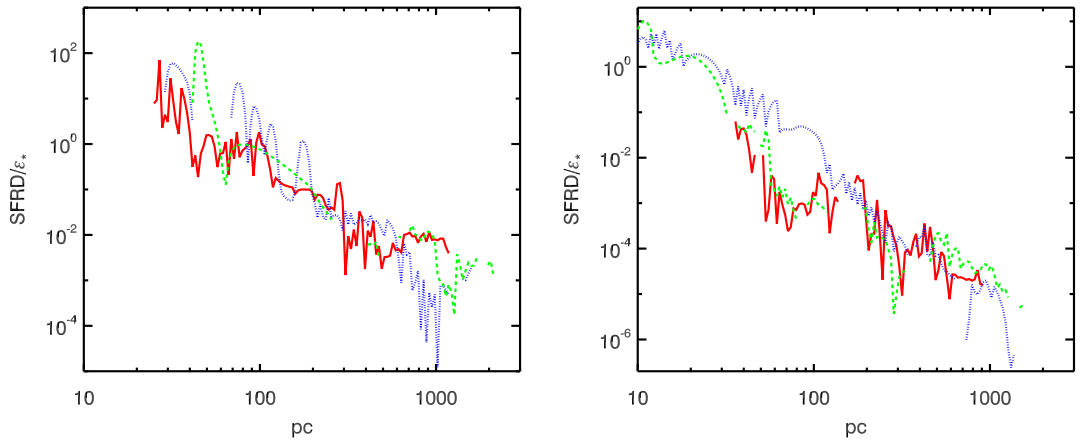

Fig. 2 The radial profiles of angle-averaged SFRD ($\dot{\rho}_*$) for the models AMR (left panel) and CMR (AMR). The solid, dotted and dashed lines correspond to the snapshots taken at t=2.235, 4.47 and 6.705 Myr, respectively. The vertical axis is $\dot{\rho}_*/\epsilon_*$ in unit of $\mathrm{M}_\odot \mathrm{yr}^{-1}(100\mathrm{pc})^{-3}$. The horizontal axis is in unit of pc. We take only the dense gas with $T < 10^5$ K in the calculation.

3.2 Gas-rich galaxies: mutually reinforced feedbacks

In this and next subsection, we explore the feedback effects by turn on/off one of the two forms of feedback. Firstly, we study the gas-rich case.

Figure 3 shows the same physical quantities as Figure 1 but for models AM (top panels) and AR (bottom panels). Radiative heating/cooling is always turned on. The difference is that one has only radiation pressure feedback and the other has only mass outflow feedback. Both models AM and AR have much weaker feedback effect in the respects of smaller effective feedback radii, fewer clumps and filaments compared with model AMR. The top panels of model AM are snapshots at time 4.47 Myr, the bottom panels present the snapshots of model AR at time 27.71 Myr. For model AM with only mass outflow feedback, the shocked shells are not symmetrical about the middle plane with $z = 0$. This is because of that at the very beginning the shocked shell above the $z = 0$ plane fragments firstly, the outflow and radiation traverse gaps of the fragmented shell and interact with the outer ISM, and then the upper bubble grows much more quickly. On the other hand, some of the blown-away gas in the upper panel would fall back down. It would be harder to blow away the gas below the equator plane. Therefore, once the asymmetry appears, the growth of asymmetry will be a runaway process. We have not shown the snapshots of model AR at time 4.47 Myr since the feedback effects only effective in the very inner regions. The luminosity which we use are designed to produce radiation pressure to balance the gravity. But why the radiation pressure seems not large enough? The reason is that the SMBH gravity is not included in the luminosity design. After long time evolution, most of the gas flow into the inner boundary along the middle-plane. We can see from the bottom panels of Figure 3 that the radiation pressure feedback influences only along the polar axis and in small regions even after long time evolution.

We can see that the effective feedback regions are almost inside the outer shell from top panels of Figure 3. As shown in the bottom panels in the same Figure, the gas temperature can be above 10^6 K which is a

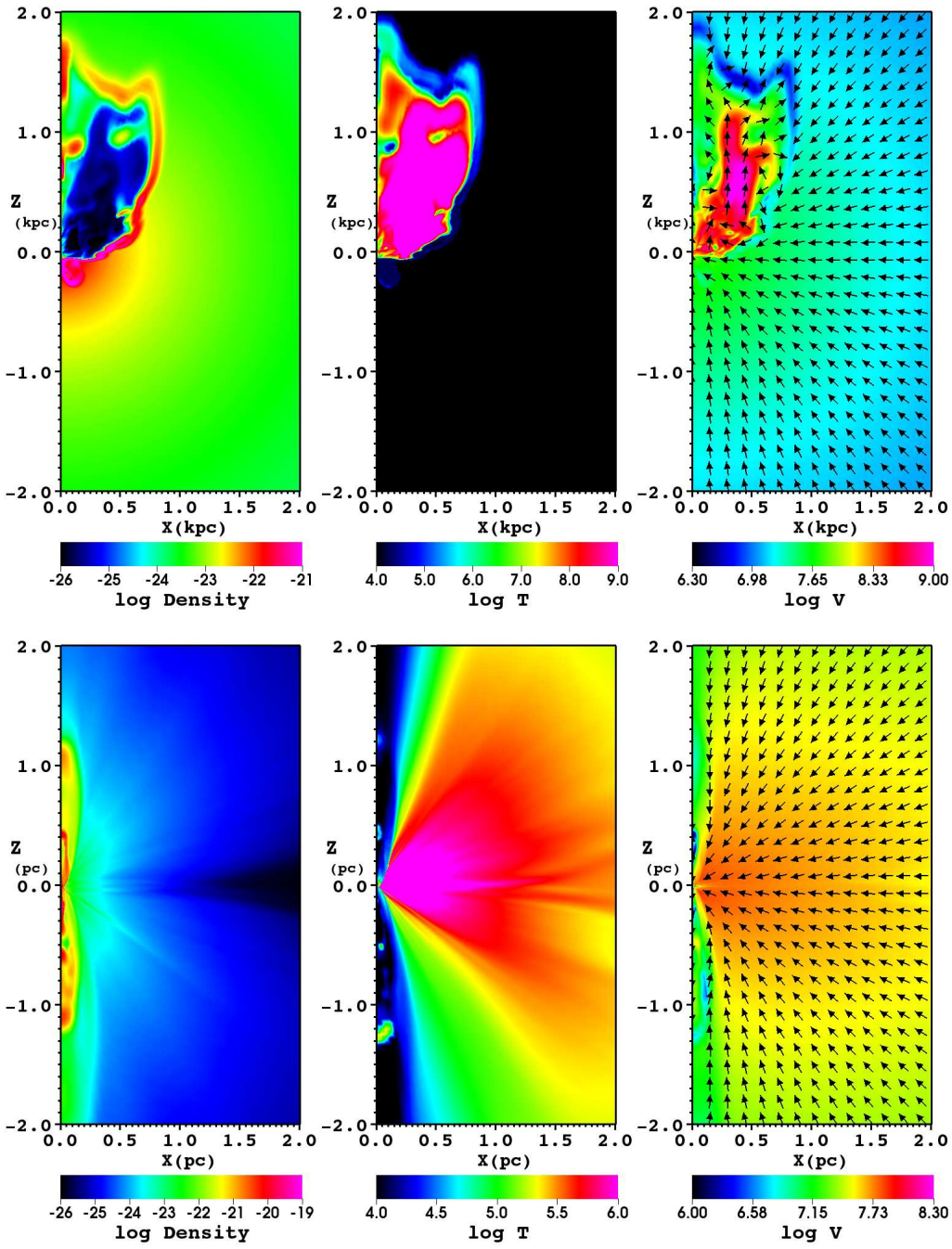

Fig. 3 Top panels: model AM with only mass outflow feedback; bottom panels: model AR with only radiative feedback. The color scales for the panels are same as they are in Figure 1. The top panels are snapshots taken at time 4.47 Myr, the bottom panels present the snapshots of model AR taken at time 27.71 Myr.

discrepancy between these two models is due to the gas density of outermost shell is so high in model AM that the shell is optically thick, while the outermost shell in model AR is still optically thin so that the photons from the central engine could penetrate the shell to heat the gas in the distance. Ciotti et al. (2010) claimed a similar conclusion that the radiative feedback is effective at relatively much larger radii.

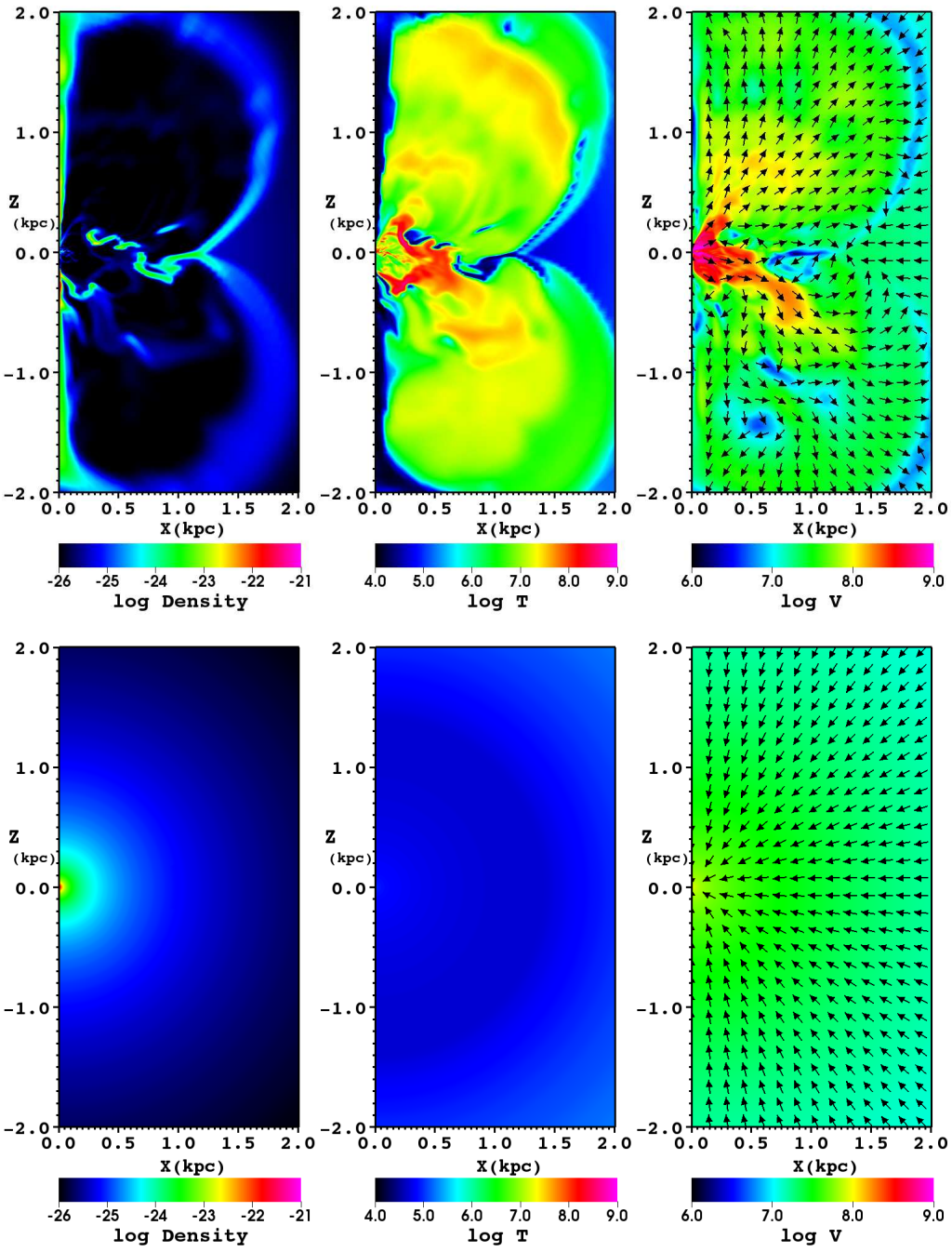

Fig. 4 Top panels: model CM with only mass outflow feedback; bottom panels: model CR with only radiative feedback. The color scales for the panels are same as they are in Figure 1. All the panels are snapshots taken at time 4.47 Myr.

are much weaker. In other words, the two types of feedbacks reinforced each other. This is because that the long-distance radiation pressure could accelerate gas very far which would reduce the resistance, so that the mass outflows propagate forward easier to impact the ISM at large radii. On the other hand, when the adjacent gas is compressed by mass outflows, the line fore would increase if the temperature is lower than 10^5 K. In general, the physics included here are very complicated. We leave the detailed analysis for a

3.3 Gas-poor galaxies: outflow feedback dominated

We turn to the gas-poor case in this subsection. The results of models CM and CR are shown in Figure 4. The figure pattern is same as Figure 3 except that all the snapshots are taken at time 4.47 Myr now. For model C series, the luminosity $L_{acc} \approx 2.2\%L_{Edd}$, it is too small to produce effective radiative feedback. There are not any radiation-driven outflows in model CR as seen in the bottom panels of Figure 3. However, the mass outflow feedback is very efficient to sweep off the ISM. Comparing the top-left panel of Figure 4 with the bottom-left panel of Figure 1, we conclude that mass outflow feedback is the dominated one. The more complicated structures of model AMR indicate that radiation pressure also plays a role in the processes of feedback-ISM interactions.

Up to now, we find both radiation pressure and mass outflow are important to the ISM evolution and the feedback processes are very complicated.

4 CONCLUSIONS AND DISCUSSION

We have done 2D HD numerical simulations considering both radiative and mass outflow feedbacks to study the positive AGN feedback. We take more intact treatment of radiative heating/cooling including Compton heating/cooling, photoionization heating/recombination cooling, bremsstrahlung and line cooling. Besides Thomson scattering, we also consider line-absorption. This is by far one of the most sophisticated simulations on positive AGN feedback topic. We primarily evaluate the SFR and SFRD in the gas shells, clumps and filaments which are believed to be the ideal places for star formation. The clumps and filaments are generated by the fragmentation of the gas shells. We find that the SFR is greatly enhanced rather than disrupted by AGN feedback as also found by Nayakshin & Zubovas (2012). We conclude that AGN feedback can be positive in the respect of increasing the SFR; both radiation and mass outflow play important roles in this SMBH-galaxy co-evolution scenario. Further, we find that although radiation pressure feedback has limited effect, when mass outflow feedback is also included, they reinforce each other.

We explore the dependence on ISM density by varying the gas fraction f_g as summarized in Table 1. We do not draw the results of model BMR because it is an intermediate model between models AMR and CMR. We set the luminosity in proportional to f_g so that the gas-rich models have higher luminosity and the gas-poor models have lower luminosity. We find that for high luminosity models, both radiation and mass outflow feedback are important, they reinforce each other. While for models with low luminosity, radiation pressure is hard to drive strong outflows, although it is still effective. That is to say the models with low luminosity are mass outflow feedback dominated. These conclusions are reasonable if we take the standard thin disc (Shakura & Sunyaev 1973) or slim disc (Abramowicz et al. 1988) to explain the high luminosity models and take radiation inefficient accretion flow (RIAF; Narayan & Yi 1994) to explain the low luminosity models, respectively. Mass outflows are found in both the luminous standard thin disc (e.g., Murray et al. 1995; Proga et al. 2000) and slim disc (e.g., Ohsuga et al. 2005; Ohsuga & Mineshige 2011) and faint RIAF (e.g., Yuan et al. 2012a,b) in the past about 15 yrs. We calculate the mass inflow rates for models AMR, BMR and CMR, their time evolutions are drawn in Figure 5. The mass inflow rates are very large and highly time varying. The reason for time varying is that some of the blown-away gas would fall

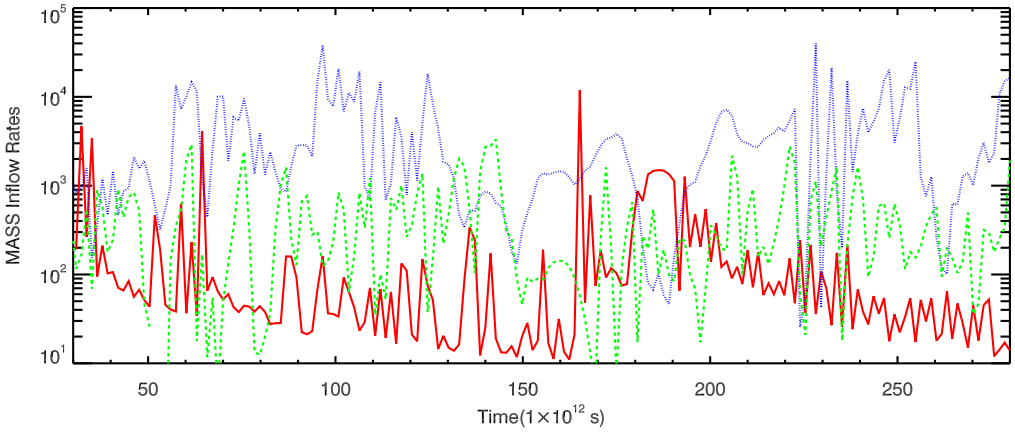

Fig. 5 The time evolution of mass inflow rates for model AMR(red, solid line), BMR(blue, dotted line) and CMR(green, dashed line). The vertical axis is in unit 10^{25} g s^{-1} $= 0.625$ M$_\odot$ yr^{-1}, the horizontal axis is in unit of 10^{12} s $= 3.17 \times 10^4$ yr.

Nayakshin & Zubovas (2012) did not evaluate AGN feedback triggered SFR, they showed the pressure in the shocked ambient gas is much larger than the maximum gas pressure in the pre-quasar host. Physically, by compressing the cold gas in the hosts, the strong pressure is able to trigger star formation or accelerate it. Ishibashi & Fabian (2012) given the SFRs of the order of $\sim 10-100\,\mathrm{M}_\odot\ \mathrm{yr}^{-1}$ for $\epsilon_* \sim 0.01-0.1$ and $f_g = 0.16$. This value is comparable to our results for model AMR. Ishibashi & Fabian (2012) considered only radiation pressure on dust, so their results are only reliable at sufficiently large radii ($r \gg GM_{BH}/\sigma^2 \approx 10$ pc; inside our simulation domain). Until now, no works calculate the SFR self-consistently, although most of them claim that the conditions for star formation are satisfied. We emphasize that taking the star formation processes into the simulations is necessary. This will be a future project.

Our treatment of accretion luminosity is not self-consistent. The star formation process is not included in the simulations. To correctly capture the accretion, feedback and star formation in a single simulation is a very formidable project. But we can treat the star formation in a semi-analytic way, and parameterize the relation between the accretion rate onto the black hole and mass inflow rate at the inner boundary. To fully understand the radiative feedback, radiation transfer simulation is needed. These improvements will be studied in future works.

Acknowledgements We thank Prof. Feng Yuan for his useful suggestions, and Dr. Tomohisa Kawashima for his thoughtful comments/suggestions. We are also very grateful to the anonymous referee for his/her informative and instructive comments. This work was supported in part by the Natural Science Foundation of China (grants 11203057, 11103061, 11133005), and the Shanghai Postdoctoral Scientific Program (grant 11R21417700). The simulations were carried out at Shanghai Supercomputer Center.

References

Abramowicz, M. A., Czerny, B., Lasota, J. P., & Szuszkiewicz, E. 1988, ApJ, 332, 646 11

Cano-Díaz, M., Maiolino, R., Marconi, A., et al. 2012, A&A, 537, L8 2

Ciotti, L., Ostriker, J. P., & Proga, D. 2009, ApJ, 699, 89 2

Ciotti, L., Ostriker, J. P., & Proga, D. 2010, ApJ, 717, 708 9

Crenshaw, D. M. 1997, in Mass Ejection from Active Galactic Nuclei, *Astronomical Society of the Pacific Conference Series*, vol. 128, edited by N. Arav, I. Shlosman, & R. J. Weymann, 121 4

Crenshaw, D. M., Kraemer, S. B., & George, I. M. 2003, ARA&A, 41, 117 4

Di Matteo, T., Springel, V., & Hernquist, L. 2005, Nature, 433, 604 2

Fabian, A. C. 2012, ARA&A, 50, 455 1, 2

Fabian, A. C., Celotti, A., & Erlund, M. C. 2006, MNRAS, 373, L16 2

Fanidakis, N., Baugh, C. M., Benson, A. J., et al. 2011, MNRAS, 410, 53 2

Fanidakis, N., Baugh, C. M., Benson, A. J., et al. 2012, MNRAS, 419, 2797 7

Farrah, D., Urrutia, T., Lacy, M., et al. 2012, ApJ, 745, 178 2

Ferrarese, L., & Merritt, D. 2000, ApJ, 539, L9 1, 5

Gebhardt, K., Kormendy, J., Ho, L. C., et al. 2000, ApJ, 543, L5 1

Hamann, F., Barlow, T., Cohen, R. D., Junkkarinen, V., & Burbidge, E. M. 1997, in Mass Ejection from Active Galactic Nuclei, *Astronomical Society of the Pacific Conference Series*, vol. 128, edited by N. Arav, I. Shlosman, & R. J. Weymann, 19 4

Hamann, F., Kaplan, K. F., Rodríguez Hidalgo, P., Prochaska, J. X., & Herbert-Fort, S. 2008, MNRAS, 391, L39 4

Hayes, J. C., Norman, M. L., Fiedler, R. A., et al. 2006, ApJS, 165, 188 4

Ishibashi, W., & Fabian, A. C. 2012, MNRAS, 427, 2998 2, 3, 7, 12

Kaastra, J. S., Mewe, R., Liedahl, D. A., Komossa, S., & Brinkman, A. C. 2000, A&A, 354, L83 4

Krongold, Y., Nicastro, F., Elvis, M., et al. 2007, ApJ, 659, 1022 4

Kurosawa, R., & Proga, D. 2009, MNRAS, 397, 1791 2, 4

Mac Low, M.-M., McCray, R., & Norman, M. L. 1989, ApJ, 337, 141 7

Marconi, A., & Hunt, L. K. 2003, ApJ, 589, L21 1

Moe, M., Arav, N., Bautista, M. A., & Korista, K. T. 2009, ApJ, 706, 525 2

Murray, N., Chiang, J., Grossman, S. A., & Voit, G. M. 1995, ApJ, 451, 498 11

Narayan, R., & Yi, I. 1994, ApJ, 428, L13 11

Nayakshin, S., & Zubovas, K. 2012, MNRAS, 427, 372 2, 3, 7, 11

Novak, G. S., Ostriker, J. P., & Ciotti, L. 2011, ApJ, 737, 26 5

Ohsuga, K., & Mineshige, S. 2011, ApJ, 736, 2 11

Ohsuga, K., Mori, M., Nakamoto, T., & Mineshige, S. 2005, ApJ, 628, 368 11

Ostriker, J. P., Choi, E., Ciotti, L., Novak, G. S., & Proga, D. 2010, ApJ, 722, 642 4

Page, M. J., Symeonidis, M., Vieira, J. D., et al. 2012, Nature, 485, 213 2

Proga, D., & Kallman, T. R. 2004, ApJ, 616, 688 4

Proga, D., Stone, J. M., & Kallman, T. R. 2000, ApJ, 543, 686 2, 3, 4, 11

Santini, P., Rosario, D. J., Shao, L., et al. 2012, A&A, 540, A109 2

Shakura, N. I., & Sunyaev, R. A. 1973, A&A, 24, 337 11

Sijacki, D., Springel, V., Di Matteo, T., & Hernquist, L. 2007, MNRAS, 380, 877 2

Silk, J., & Nusser, A. 2010, ApJ, 725, 556 2

Silk, J., & Rees, M. J. 1998, A&A, 331, L1 2

Springel, V., Di Matteo, T., & Hernquist, L. 2005, MNRAS, 361, 776 2

Stevens, I. R., & Kallman, T. R. 1990, ApJ, 365, 321 3

Stone, J. M., & Norman, M. L. 1992, ApJS, 80, 753 4

Sturm, E., González-Alfonso, E., Veilleux, S., et al. 2011, ApJ, 733, L16 2

Tombesi, F., Cappi, M., Reeves, J. N., & Braito, V. 2012, MNRAS, 422, L1 4

Tombesi, F., Cappi, M., Reeves, J. N., et al. 2010, A&A, 521, A57 4

Tombesi, F., Cappi, M., Reeves, J. N., et al. 2011, ApJ, 742, 44 4

van Dokkum, P. G., Whitaker, K. E., Brammer, G., et al. 2010, ApJ, 709, 1018 2

Vishniac, E. T. 1983, ApJ, 274, 152 7

Yuan, F., Bu, D., & Wu, M. 2012a, ApJ, 761, 130 11

Yuan, F., Wu, M., & Bu, D. 2012b, ApJ, 761, 129 11